A model of larval biomechanics reveals exploitable passive properties for efficient locomotion

A model of larval biomechanics reveals exploitable passive properties for efficient locomotion

Dylan Ross[1], Konstantinos Lagogiannis[1], Barbara Webb[1]

School of Informatics, University of Edinburgh,
10 Crichton St, Edinburgh EH8 9AB, UK.
dylan.martin.ross@gmail.com,{klagogia,bwebb}@inf.ed.ac.uk

Abstract. To better understand the role of natural dynamics in motor control, we have constructed a mathematical model of crawling mechanics in larval *Drosophila*.
The model accounts for key anatomical features such as a segmentally patterned, viscoelastic outer body wall (cuticle); a non-segmented inner cavity (haemocoel) filled with incompressible fluid that enables visceral pistoning; and claw-like protrusions (denticle bands) giving rise to asymmetric friction.
Under conditions of light damping and low forward kinetic friction, and with a single cuticle segment initially compressed, the passive dynamics of this model produce wave-like motion resembling that of real larvae. The presence of a volume-conserving hydrostatic skeleton allows a wave reaching the anterior of the body to initiate a new wave at the posterior, thus recycling energy. Forcing our model with a sinusoidal input reveals conditions under which power transfer from control to body may be maximised. A minimal control scheme using segmentally localised positive feedback is able to exploit these conditions in order to maintain wave-like motion indefinitely. These principles could form the basis of a design for a novel, soft-bodied, crawling robot.

Keywords: larval Drosophila, biomechanical model, positive feedback control, peristaltic motion.

1 Introduction

Felicitous use of mechanics can reduce the computational and energetic burdens faced by artificial and biological agents. As an extreme case, the passive dynamic walkers of McGeer were capable of producing naturalistic walking behaviour in the absence of any active control system and using only the energy provided by moving down a slight incline [1]. More recently, robotics has started to move beyond the confines of rigid body mechanics to exploit characteristically soft

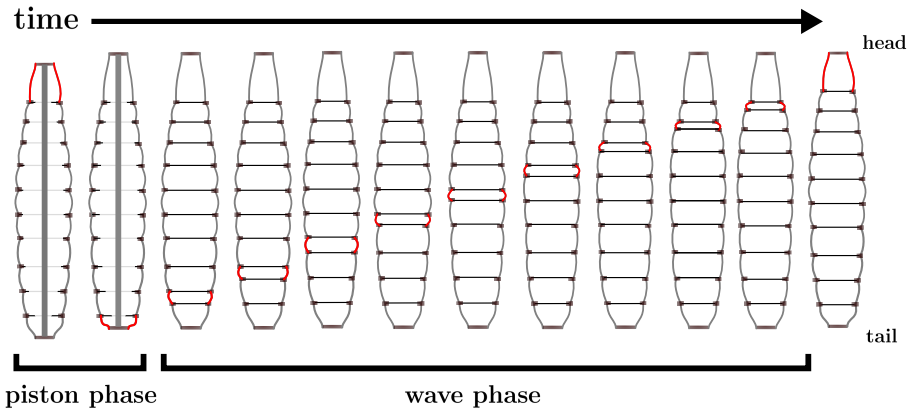

Fig. 1. crawling in larval *Drosophila* : *Drosophila* larvae crawl using a two-phase visceral pistoning mechanism. During piston phase the head, tail, viscera, and coelomic fluid move forward in tandem. Then, during wave phase, a longitudinal wave of segment compression travels from the posterior to anterior of the body.

or compliant phenomena to produce complex mechanical outputs in response to simple control inputs [2, 3]. Biology can provide crucial insights for designing such systems, as complex biological control problems are often simplified or solved by body mechanics rather than requiring precisely orchestrated neural control [4, 5].

Larval *Drosophila melanogaster*, a tiny organism with a nervous system of less than 10,000 neurons, is an excellent example. The larva's primary goal is to acquire and store enough energy to successfully pupate and become a fruitfly; hence its locomotion should be as energy efficient as possible. The *Drosophila* larva possesses a hydrostatic skeleton that runs the entire length of its body and is surrounded by a segmentally patterned cuticle and musculature. Kinematic evidence suggests that it moves using a two-phase *visceral pistoning* mechanism similar to that observed in *Manduca sexta* caterpillars [6, 7] (Figure 1). During *piston phase*, the head, tail, and viscera of the organism move forward in a single step. Then, during *wave phase*, a travelling wave of compression propagates from the posterior to the anterior of the animal, moving each segment forwards in sequence. When the travelling wave reaches the head, this process repeats.

Notably, the propagation speed and cycle period of peristaltic waves is highly stereotyped [7, 8]. *Drosophila* locomotion differs from that of *Manduca* in that the larva lacks hydrostatic prolegs, and lifts very little from the substrate during crawling [8]. This is reflected by a very low number of circumferential relative to longitudinal muscle fibres in *Drosophila* [9]. Motor neuron recordings show that all muscles within a segment are activated simultaneously during fictive crawling [10], suggesting that the *Drosophila* larva may use an especially simple control scheme to direct crawling behaviour.

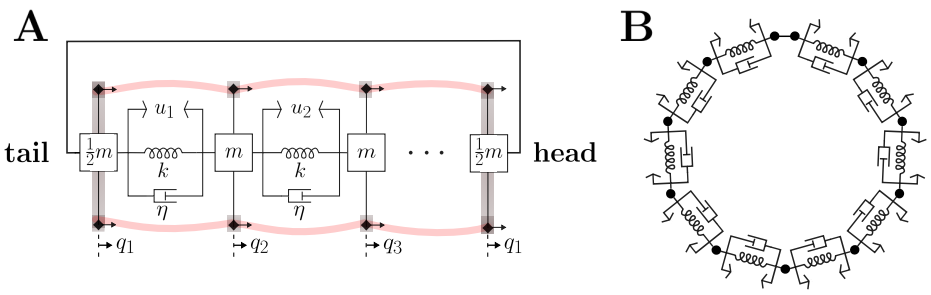

Fig. 2. model schematic : **A** we model the segmented cuticle of the *Drosophila* larva as a set of coupled spring-mass-damper systems subject to an asymmetric Coulomb friction force. Volume-conserving coelomic fluid is incorporated as a rigid link connecting the head and tail masses. **B** The presence of this rigid link means that our model has a ring topology.

We have defined a one-dimensional mechanical model to explore how physical properties of the larval body may simplify its control. We examine why the larva may generate peristaltic waves with a constant period, and how peristalsis may be maintained by a minimal control scheme. Unfortunately, there is little available experimental data regarding the mechanical properties of larval tissues. We therefore constructed our model in accordance with known anatomy and kinematics.

2 Model construction

A general practice in modelling soft tissues is to use idealized mass-spring-damper systems [11–14].

Following this approach, we represent the head, tail, and segmental boundaries as 11 point masses, m_i, constrained to move along a single direction parallel to the plane of the substrate. The time varying positions q_i and velocities $\dot{q}_i$ of the masses along this direction of travel describe the state of our model. During peristalsis, the cuticle undergoes reversible viscoelastic strain, modelled here as an ideal spring and damper connected in parallel between neighbouring pairs of masses, characterised by a spring constant, k, and damping constant, η.

Very little change in axial or radial dimensions is observed during larval locomotion [7, 8], suggesting that coelomic fluid may be modelled as an incompressible liquid which prevents changes in total body volume. This is enforced in our model by connecting the head and tail masses by a rigid link, which imposes the constraint $\dot{q}_1 = \dot{q}_{11} \; \forall \, t$.

Each body segment in the *Drosophila* larva contacts the substrate via a band of hard, claw-like projections called denticles. Since denticles extend primarily in the posterior direction,we model their interaction with the environment as a directionally asymmetric Coulomb friction force:

$$F_i(\mathbf{q}, \dot{\mathbf{q}}, \mathbf{u}) = \begin{cases} -\mu_{f:b}\mu_{k:s}\mu mg & \text{if } \dot{q}_i > 0 \ \vee \ F_{\text{ext},i} > \mu_{f:b}\mu mg \\ \mu_{k:s}\mu mg & \text{if } \dot{q}_i < 0 \ \vee \ F_{\text{ext},i} < -\mu mg \\ -F_{\text{ext},i} & \text{if } \dot{q}_i = 0 \ \wedge \ -\mu mg \leq F_{\text{ext},i} \leq \mu_{f:b}\mu mg \end{cases} \tag{1}$$

where g is standard gravity, μ is a coefficient of static friction specific to the denticle bands and the substrate, $\mu_{k:s}$ is the ratio of kinetic to static friction, and $\mu_{f:b}$ is the ratio of friction in the forward direction to friction in the backward direction. $F_{\text{ext},i}$ is the total non-frictive force being applied to the i-th mass.

As input to our model we allow time-varying tensions, representing muscle forces, to develop between neighbouring masses. We denote the vector of muscle tensions as $\mathbf{u}^{\mathrm{T}} = [u_1, u_2, \cdots, u_N]$ and impose the constraint $0 \leq \mathbf{u} \leq d$ to represent the fact that muscle forces saturate and are purely tensile in nature. A gain parameter $b \geq 0$ allows scaling of $\mathbf{u}$ to an appropriate range for the model's passive forces.

Assembling these elements gives the model shown in Figure 2. Isolating the forces exerted on each mass and applying Newton's second law gives a system of N second-order differential equations which must be solved for q_i and $\dot{q}_i$

$$\mathbf{M}\ddot{\mathbf{q}} = -k\mathbf{D}_2\mathbf{q} - \eta\mathbf{D}_2\dot{\mathbf{q}} + b\mathbf{D}_1\mathbf{u} + \mathbf{F} \tag{2}$$

where $\mathbf{M}$ is the $N \times N$ inertia matrix, $\mathbf{D}_2$ is an $N \times N$ circulant second difference matrix describing the coupling between the head, tail, and segment boundaries, and $\mathbf{D}_1$ is an $N \times N$ circulant backward difference matrix that describes how a particular muscle tension will pull one segment backwards and another forwards

$$\mathbf{M} = \begin{bmatrix} m & & & & \\ & m & & & \\ & & \ddots & & \\ & & & m & \\ & & & & m \end{bmatrix} \quad \mathbf{D}_2 = \begin{bmatrix} 2 & -1 & & & -1 \\ -1 & 2 & -1 & & \\ & \ddots & \ddots & \ddots & \\ & & -1 & 2 & -1 \\ -1 & & & -1 & 2 \end{bmatrix} \quad \mathbf{D}_1 = \begin{bmatrix} 1 & & & & -1 \\ -1 & 1 & & & \\ & \ddots & \ddots & & \\ & & & -1 & 1 \end{bmatrix} \tag{3}$$

By introducing spatial and temporal scaling, we can reduce the dimensionality of our parameter space and highlight useful physical relationships.

Letting $\boldsymbol{\chi}$ denote the nondimensionalised position vector, the scaled dynamics may be written

$$\ddot{\boldsymbol{\chi}} = -\mathbf{D}_2\boldsymbol{\chi} - 2\zeta\mathbf{D}_2\dot{\boldsymbol{\chi}} + \mathbf{D}_1\mathbf{u} + \mathbf{G}(\mathbf{x}, \mathbf{u}) \tag{4}$$

where the damping ratio $\zeta = \eta/2\sqrt{km} \geq 0$ specifies the ratio of viscous to elastic and inertial forces. $\mathbf{G}$ denotes the nondimensionalised friction function

$$G_i(\boldsymbol{\chi}, \dot{\boldsymbol{\chi}}, \mathbf{u}) = \begin{cases} -\gamma_{f:b}\gamma_{k:s}\gamma & \text{if } \dot{q}_i > 0 \ \vee \ \frac{1}{b}F_{\text{ext},i} > \gamma_{f:b}\gamma \\ \gamma_{k:s}\gamma & \text{if } \dot{q}_i < 0 \ \vee \ \frac{1}{b}F_{\text{ext},i} < -\gamma \\ -\frac{1}{b}F_{\text{ext},i} & \text{if } \dot{q}_i = 0 \ \wedge \ -\gamma \leq \frac{1}{b}F_{\text{ext},i} \leq \gamma_{f:b}\gamma \end{cases} \tag{5}$$

The parameter $\gamma = \mu mg/b$ determines the magnitude of static friction in the backward direction. We have rewritten $\gamma_{f:b} = \mu_{f:b}$ and $\gamma_{k:s} = \mu_{k:s}$ for notational completeness. The details of this non-dimensionalisation process are provided in the supplementary material [21].

3 Results

We solved (4) using a fixed-step forward Euler method. Integration accuracy was assessed by calculating the summed kinetic, potential, and dissipated energy in our model system over the domain of integration. We tuned the integration timestep until error in total energy fell below 1%, finding a timestep of $10^{-3}t_c$ to be sufficient.

3.1 Passive Dynamics of a Single Segment; Role of Model Parameters

To explore the role of the parameters $\zeta, \gamma, \gamma_{f:b}$, and$\gamma_{k:s}$, we first examined the behaviour of a single segment boundary under the influence of passive mechanical forces. We simplified our analysis by assuming that all other segment boundaries were held fixed to the substrate, enforced by the constraint $\ddot{\chi}_{i\neq j} = 0$, where j specifies the freely moving segment boundary. To reflect the fact that motion of an isolated segment boundary would normally occur within the context of an ongoing peristaltic wave (Figure 1), we set initial conditions such that the free segment boundary was initially at rest away from equilibrium, in an extreme posterior or anterior position (Figure 3A, left panel, $\tau = 0$).

Passive viscoelastic and friction forces alone were able to produce trajectories that qualitatively match movements observed in the real larva (Figure 3A, left panel). Elastic forces exerted by the cuticle initially accelerate the segment boundary towards the cuticle's equilibrium position, which corresponds to the minimum of the elastic potential energy function shown in Figure 3A (right panel). Motion of the segment boundary is opposed by viscous damping and kinetic friction forces, which slow the segment boundary and eventually bring it to rest. Increasing the parameter ζ causes an increase in the magnitude of viscous forces, decreasing segment boundary velocity. When $\zeta < 1$, the moving mass may overshoot the cuticle's equilibrium position before coming to rest. Conversely, $\zeta \geq 1$ implies that the mass will move slowly towards equilibrium without overshoot (Figure 3A, left panel). Examining (5), we see that $\gamma_{k:s}\gamma$ sets the magnitude of kinetic friction when the segment boundary is moving in the posterior direction, and $\gamma_{f:b}$ scales this quantity to specify the magnitude of

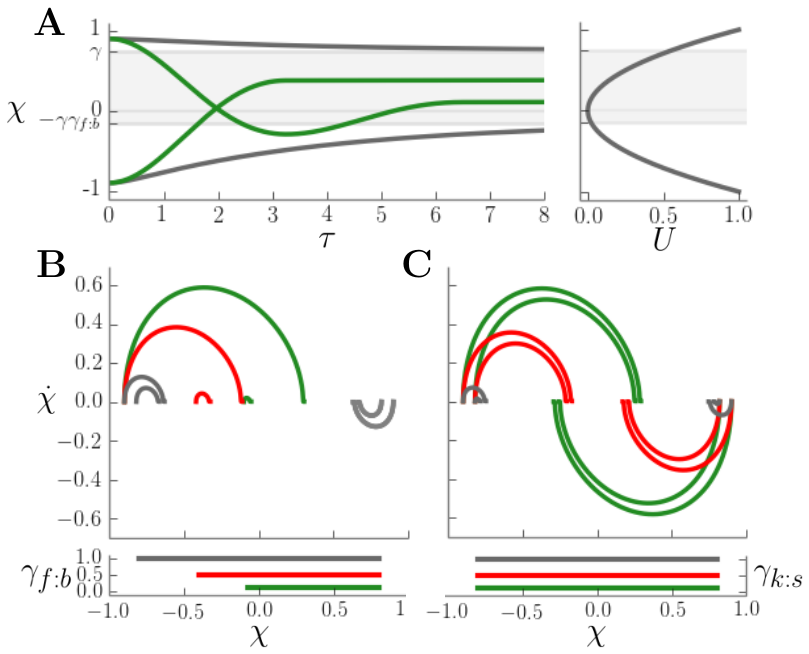

Fig. 3. passive dynamics of a single segment : A (left) evolution of segment boundary position for $\zeta = 2$ (black) or $\zeta = 0.25$ (green), with $\gamma = 0.9$, $\gamma_{f:b} = 0.4$, $\gamma_{k:s} = 0.1$. (right) elastic energy stored in the cuticle as a function of segment boundary displacement. Shading indicates the range of positions stabilised by static friction. **B** (top) position-velocity phase trajectories for $\gamma_{f:b} = 0.1$ (green), 0.5) (red), or 1.0 (gray). Trajectories with negative velocity are unaffected by change in $\gamma_{f:b}$. (bottom) range of positions stabilised by static friction for these values of $\gamma_{f:b}$. **C** (top) phase trajectories for $\gamma_{k:s} = 0.1$ (green), 0.5 (red), or 1.0 (gray). (bottom) range of positions stabilised by static friction for these values of $\gamma_{k:s}$.

forward kinetic friction. Accordingly, changing $\gamma_{k:s}$ results in directionally symmetric scaling of segment boundary velocity and final displacement (Figure 3C), while changing $\gamma_{f:b}$ allows directionally asymmetric scaling (Figure 3B).

When the segment boundary comes to rest, static friction may hold it in place. By inspection of (5), γ sets the maximum magnitude of static friction in the posterior direction while $\gamma_{f:b}$ multiplies this quantity to give the maximum magnitude in the anterior direction. The expression $\gamma_{f:b}\gamma \leq \chi \leq \gamma$ thus specifies a stable range of positions in which static friction forces completely oppose elastic forces. A mass at rest within this region will remain at rest (Figure 3A, B, C).

Though the range of possible values for $\zeta, \gamma, \gamma_{f:b}$, and$\gamma_{k:s}$ is very large, we focus on the following cases:

1. $\gamma = 0.9$ and $\gamma_{k:s} = 0.9$ or 0.1, i.e. kinetic friction is either equal to, or far weaker than, maximum static friction. The first case would correspond to

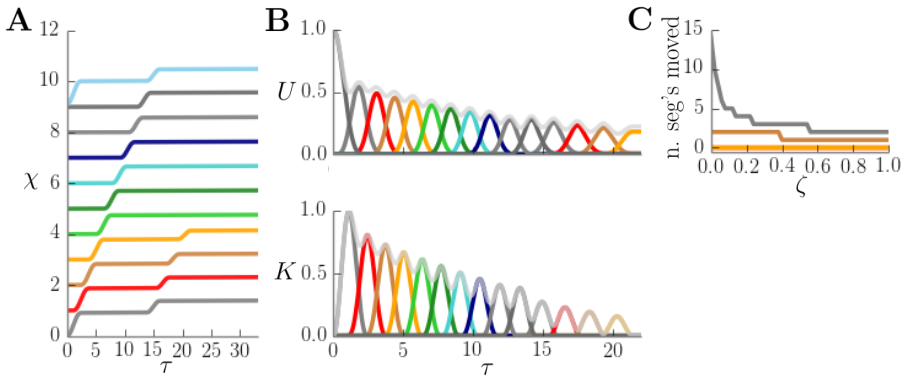

Fig. 4. passive dynamics of the full body model : A segment boundary displacements in the absence of muscle tension, with $\zeta = 0$, $\gamma = 0.9$, $\gamma_{f:b} = 0.9$, $\gamma_{k:s} = 0.1$. **B** elastic energy stored in each cuticle segment (top, U) and kinetic energy of each segment boundary (bottom, K) during the wave shown in **A**. **C** number of discrete segment boundary movements during a passive peristaltic wave as a function of ζ, for friction conditions $\gamma_{k:s} = 0.1$, $\gamma_{f:b} = 0.4$ (gray), $\gamma_{k:s} = 0.9$, $\gamma_{f:b} = 0.4$ (brown), $\gamma_{k:s} = 0.1$, $\gamma_{f:b} = 1.0$ (orange), $\gamma_{k:s} = 0.9$, $\gamma_{f:b} = 1.0$ (orange).

the larva "dragging" its denticle bands across the substrate; the latter to lifting the denticles as they move.

2. $\gamma_{f:b} = 1.0$ or 0.4, i.e. either symmetrical friction, or higher backward than forward friction, which could result from denticle orientation [15].
3. $\zeta \in [0, 0.25, 0.5, 1.0, 2.0]$: a representative set of damping ratios which ranges from zero viscous damping to heavily overdamped

3.2 Passive Dynamics of the Whole Body

Using the full model (4), we next examined the role of passive mechanics in locomotion. We set initial conditions such that the head segment was almost fully compressed, storing elastic energy. We then integrated our model equations in the absence of active muscle tensions, and observed the passive response of the system.

Under particular parameter choices, our model is capable of producing completely passive peristaltic waves (Figure 4A). In particular, with asymmetric friction forces ($\gamma_{f:b} = 0.4$), low kinetic friction ($\gamma_{k:s} = 0.1$), and low viscous damping ($\zeta < 0.6$), a wave may propagate from posterior to anterior while moving the body across the substrate (Figure 4C). The elastic energy stored in the compressed head segment is converted to kinetic energy as the segment expands. The asymmetry in our friction function means that expansion occurs through forward movement of the head, and due to the rigid link constraint (representing volume conservation of the internal coloemic fluid) this causes compression of the tail segment. The tail segment in turn expands forward, transferring energy

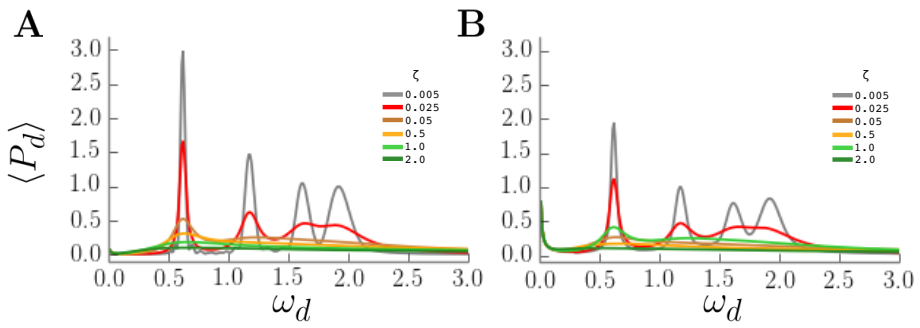

Fig. 5. resonant frequencies : A Frictionless system with $\zeta \in \{0.005, 0.025, 0.05, 0.5, 1, 2\}$; shows peak resonant frequencies with power going lower as damping ζ increases. Increasing damping ζ drops the peak power and makes the tuning wider. (In the non-dimensionalized system units are $\frac{F_d t_c}{m}$) **B** adding friction does not affect the location of the resonant frequencies but does reduce the amount of power absorbed, without broadening the spectrum of peak responses. Friction also adds an efficient mode close to zero frequency.

to the neighbouring segment boundary, and the process continues. Since friction and viscous damping dissipate an amount of energy each time a segment boundary moves, the travelling wave is gradually attenuated. Nevertheless, if dissipative forces are sufficiently low, the energy supplied by compressing the head segment may propagate through the entire body and even "loop" again from head to tail (Figure 4A). This phenomenon is possible due to hydrostatic coupling between the head and tail, and is prevented by removing the rigid link constraint in our model. Our analysis suggests a view of the larval body as a ring of energy storage devices with rectified, dissipative connections (Figure 2B).

3.3 Resonance and Preferred Input Timing

We next examined the response of our system to energy input by applying sinusoidal forcing to the tail mass. The work done by a force F_d acting upon a mass to move it a distance dq is given by $dW = F_d dq$. The rate of this process gives the power supplied $P_d = F_d \dot{q}$. Thus, the power provided by applying sinusoidal forcing to the tail mass in the non-dimensionlized system is

$$P_d = \frac{F_d t_c}{m} \cos(\omega_d \tau) \frac{d\chi}{d\tau}. \tag{6}$$

Note that direction and timing of input force are important as power is maximised when force is in phase with velocity $\dot{\chi}$. In general the driving force may add or remove energy during different parts of the cycle and the two may balance, giving on average $\langle P_d(\omega_d) \rangle = 0$ for driving frequency ω_d.

We predicted that in order to maximise energy input, our stimulation frequency would have to relate to the body's passive properties, that define $\dot{\chi}$.

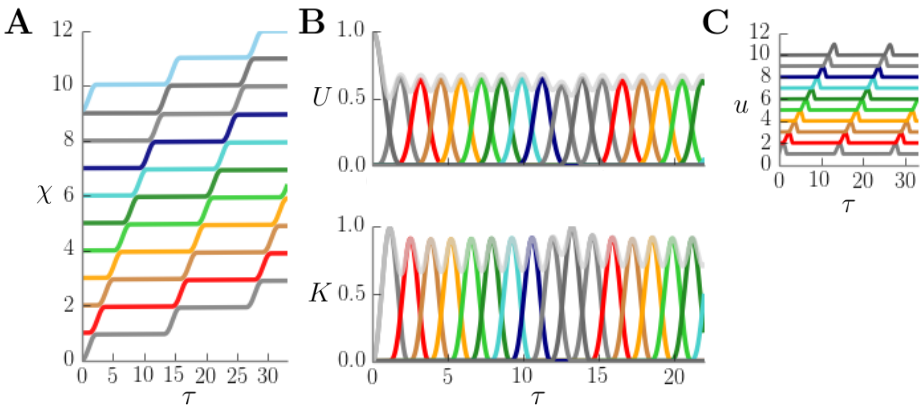

Fig. 6. local positive feedback control : A segment boundary displacements under positive feedback control (gain $\beta = 0.105$, parameter choices as in Figure 4A). **B** elastic energy stored in each segment (top) and kinetic energy of each segment boundary (bottom) during **A**. **C** muscle tensions produced by the positive feedback control law (7) during **A**. Tensions have been normalized and offset for presentation.

Indeed, it is a well known property of n spring-coupled masses to exhibit N (possibly redundant) resonant frequencies at which energy absorption is maximized. Figure 5A shows the average $\langle P_d(\omega_d) \rangle$ power supplied by the driving force, numerically evaluated over 10^2 cycles at frequency ω_d in the absence of friction forces. With low damping coefficient ζ, four peaks are evident. The location of these peaks has been verified by an analysis of the normal modes of our system (not shown).

In the frictionless case, viscous damping is the only dissipative force. Increasing damping reduces and broadens the peaks of power absorption. Introducing asymmetric friction decreases the amplitude of the peaks without simultaneous broadening, and also adds a peak towards low frequencies (Figure 5B). The increase in efficiency at low driving frequencies comes due to the reduction of the higher derivatives making the velocity of the driven mass effectively in phase with the driving force as it is dragged against the friction. If the driving force is provided by muscle activation then we can conclude the timing of muscle activation is important in order to achieve efficient locomotion, and this becomes even more evident as damping is decreased.

3.4 Generating Locomotion Through Local Positive Feedback

We constructed a control scheme that would exploit our model's passive dynamics in order to generate forward locomotion. This controller uses segmentally localised positive feedback of cuticle strain rate to produce muscle tensions according to the control law:

$$\mathbf{u} = \beta \mathbf{D}_1^{\mathrm{T}} \dot{\boldsymbol{\chi}} \qquad 0 \leq \mathbf{u} \leq d \tag{7}$$

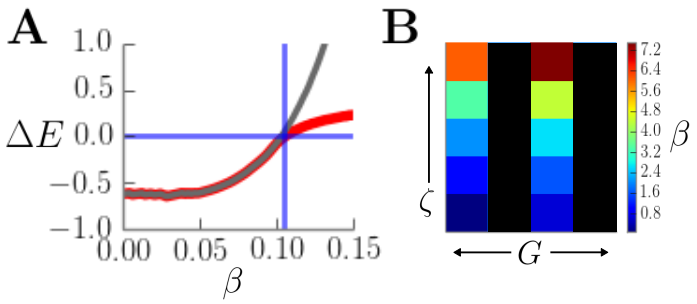

Fig. 7. tuning feedback gain : A change in total elastic and kinetic energy (ΔE) as feedback gain β is varied (parameters as in Figure 4A). β may be tuned to achieve zero change in total energy (blue lines). With non-saturating muscle tensions, ΔE increases exponentially with β (gray line, $d = \infty$). Decreasing maximum muscle tension d causes ΔE to saturate as β increases (red line, $d = 0.1$). **B** β required to achieve continuous locomotion under various damping conditions. Friction varies left to right as ($\gamma_{k:s} = 0.1$, $\gamma_{f:b} = 0.4$), ($\gamma_{k:s} = 0.1$, $\gamma_{f:b} = 1.0$), ($\gamma_{k:s} = 0.9$, $\gamma_{f:b} = 0.4$), ($\gamma_{k:s} = 0.9$, $\gamma_{f:b} = 1.0$). ζ increases from bottom to top as $[0.0, 0.25, 0.5, 1.0, 2.0]$. Conditions are coloured black if no value of β was able to produce continuous locomotion.

which can be interpreted as producing muscle tension across a segment in proportion to the rate at which the segment is shortening, parametrised by the strain rate-tension gain β. Substituting this definition for $\mathbf{u}$ into (4) gives the closed-loop system

$$\ddot{\boldsymbol{\chi}} = -\mathbf{D}_2\boldsymbol{\chi} - 2\zeta\mathbf{D}_2\dot{\boldsymbol{\chi}} + \beta\mathbf{D}_1\mathbf{D}_1^{\mathrm{T}}\dot{\boldsymbol{\chi}} + \mathbf{G} \tag{8}$$

Noting that $\mathbf{D}_1\mathbf{D}_1^{\mathrm{T}} = \mathbf{D}_2$ lets us rewrite this as

$$\ddot{\boldsymbol{\chi}} = -\mathbf{D}_2\boldsymbol{\chi} + (\beta - 2\zeta)\mathbf{D}_2\dot{\boldsymbol{\chi}} + \mathbf{G} \tag{9}$$

This control can be thought of as actively amplifying any passively occurring segment strain, mitigating the effects of dissipative forces and counteracting the attenuation of passive waves described above. Inspection of the closed-loop system (9) shows that as β increases, local positive feedback first acts to cancel viscous damping forces. Increasing β further effectively introduces a positive damping term, which can offset frictional losses. Tuning β allowed us to produce continuous, naturalistic, wave-like locomotion with near-constant total body energy across a range of damping and friction conditions (Figures 6, 7).

Note, however, that this controller cannot produce waves in the absence of passive body motion. If the environment is too frictive, or the head and tail are decoupled, positive feedback fails to produce continuous locomotion.

4 Discussion

We have constructed the first model of crawling mechanics in larval *Drosophila*. The model contains key anatomical features such as a segmentally patterned, viscoelastic cuticle; a non-segmented hemocoel filled with an incompressible fluid that enables visceral pistoning; and asymmetrically frictive denticle bands. Under conditions of light damping and low forward kinetic friction, the passive dynamics of this model naturally produce wave-like motion resembling that of real larvae. Using localised positive feedback of strain rate to produce muscle tensions results in a control that is matched to the passive dynamics of the body and permits an elegant, distributed implementation.

Our model provides insight into the generation of behaviour in larval *Drosophila*. For instance, the propagation speed of peristaltic waves and thus the overall speed of locomotion are highly stereotyped within a given experimental setup [7, 8]. Our model suggests that this is due to the existence of resonant modes within the larval body that may be exploited to minimize the energetic costs of locomotion. Locomotion speed has been observed to vary with substrate composition as well as denticle structure [16, 17]. Increase in speed over hard substrates has been suggested to represent an escape behaviour in response to undesirable conditions [16], but our model suggests that it may simply represent a change in the frictive forces experienced by the cuticle and denticle bands.

We stress that it is unlikely that crawling behaviour in the real larva is entirely controlled by decoupled, local positive feedback, since propagating waves of motor neuron activity persist in completely isolated nervous system preparations [10]. Positive feedback may still be used to align ongoing neural motor control signals with the mechanics of the body and environment. This is consistent with the observation that waves of muscle activation travel slower in larvae which have been experimentally deprived of mechanosensory input [18, 19].

Future work may investigate locomotion in two or three dimensions. This could be accomplished by adding revolute joints and torsional springs at each of the masses in the current model. This would enable investigation of turning in addition to linear crawling, the two key behaviours involved in larval navigation [20]. Of particular interest is whether positive feedback of strain rate can produce both behaviours.

The model and control schemes presented in this paper may serve as the basis for an efficient crawling robot able to exploit its passive dynamics in order to reduce the energetic and computational burden of control.

References

1. McGeer, T.: Passive Dynamic Walking. *The international journal of robotics research*, 62(82):62–82, (1990).
2. Hauser, H., Ijspeert, A.J., Füchslin, R.M., Pfeifer, R., Maass, W.: Towards a theoretical foundation for morphological computation with compliant bodies *Biological cybernetics*, (2011):355–370, (2012).

3. Shepherd, R.: Multigait soft robot. *Proceedings of the National Academy of Sciences of the United States of America*, 108(51):20400–3, (2011).
4. Tytell, E.D., Holmes, P., Cohen, A.H.. Spikes alone do not behaviour make: Why neuroscience needs biomechanics. *Curr Opin Neurobiol*, 21(5):816–822, (2011).
5. Kier, W.M.: The diversity of hydrostatic skeletons. *The Journal of experimental biology*, 215(Pt 8):1247–57, (2012).
6. Simon, M.A., Woods, W.A., Serebrenik, Y.V., Simon, S.M. van Griethuijsen, L.I., Socha, J.J., Lee, W.K., Trimmer, B.A.: Visceral-locomotory pistoning in crawling caterpillars. *Current biology : CB*, 20(16):1458–63,(2010).
7. Heckscher, E.S., Lockery, S.R., Doe, C.Q.: Characterization of Drosophila larval crawling at the level of organism, segment, and somatic body wall musculature. *The Journal of neuroscience*, 32(36):12460–71, (2012).
8. Berrigan, D., Pepin, D.J.: How Maggots Move: Allometry and Kinematics of Crawling in Larval Diptera *J. Insect Physiol.*, 41:(4) 329–337, (1995).
9. Landgraf, M., Bossing, T., Technau, G.M., Bate, M.: The origin, location, and projections of the embryonic abdominal motorneurons of *Drosophila*. *The Journal of neuroscience : the official journal of the Society for Neuroscience*, 17(24):9642–55, (1997).
10. Fox, L.E., Soll, D.R., Wu, C.: Coordination and modulation of locomotion pattern generators in Drosophila larvae: effects of altered biogenic amine levels by the tyramine beta hydroxlyase mutation. *The Journal of Neuroscience*, 26(5):1486–1498, (2006).
11. Boyle, J.H., Berri, S., Cohen, N.: Gait Modulation in C. elegans: An Integrated Neuromechanical Model. *Frontiers in computational neuroscience*, 6(March):10, (2012).
12. Fung, Y.C.: Biomechanics: Mechanical Properties of Living Tissues. *New York, NY*, (1993).
13. Skierczynski, B.A., Wilson, R.J., Kristan, W.B., Skalak, R.: A model of the hydrostatic skeleton of the leech. *Journal of theoretical biology*, 181(4):329–42, (1996).
14. Alscher, C.: Simulating the motion of the leech : A biomechanical application of DAEs. *Numerical Algorithms*, 19:1–12, (1998).
15. Alexandre, C.: Cuticle Preparation of Drosophila Embryos and Larvae. In C. Dahmann, editor, *Methods in Molecular Biology : Drosophila : Methods and Protocols*, Ch. 11, pages 197–205. Humana Press Inc., (2008).
16. Apostolopoulou, A.A., Hersperger, F., Mazija, L., Widmann, A., Wüst, A., Thum, A.S.: Composition of agarose substrate affects behavioral output of Drosophila larvae. *Frontiers in behavioral neuroscience*, 8(January):11, (2014).
17. Inestrosa, N.C., Sunkel, C.E., Arriagada, J., Garrido, J., Herrera, R.G.: Abnormal development of the locomotor activity in yellow larvae of *Drosophila*: a cuticular defect? *Genetica*, 97:205–210, (1996).
18. Hughes, C.L., and Thomas, J.B.: A Sensory Feedback Circuit Coordinates Muscle Activity in *Drosophila*, *Mol Cell Neurosci*, 35(2):383–396, (2007).
19. Inada, K., Kohsaka, H., Takasu, E., Nose, A.: Optical dissection of neural circuits responsible for *Drosophila* larval locomotion with halorhodopsin, *PloS one*, 6(12): 1–10, (2011).
20. Lahiri, S., Shen, K., Klein, M., Tang, A., Kane, E., Gershow, M., Garrity, P., Samuel, A.: Two alternating motor programs drive navigation in *Drosophila* larva, *PloS one*, 6(8):1–12, (2011).
21. Ross, D., Lagogiannis, K., Webb, B.: Online supplementary material, `http://maggot.eu/documents/2015/04/SuppMechBodymodel.pdf`.